ACCOUNTS
of chemical research

# *In Situ* Solid-State NMR Spectroscopy of Electrochemical Cells: Batteries, Supercapacitors, and Fuel Cells

FRÉDÉRIC BLANC,[†,‡] MICHAL LESKES,[†] AND CLARE P. GREY[*,†,§]

[†]*Department of Chemistry, University of Cambridge, Lensfield Road, Cambridge CB2 1EW, United Kingdom,* [‡]*Department of Chemistry, Stephenson Institute for Renewable Energy, University of Liverpool, Crown Street, Liverpool L69 7ZD, United Kingdom, and* [§]*Department of Chemistry, Stony Brook University, Stony Brook, New York 11790-3400, United States*

RECEIVED ON JANUARY 28, 2013

## CONSPECTUS

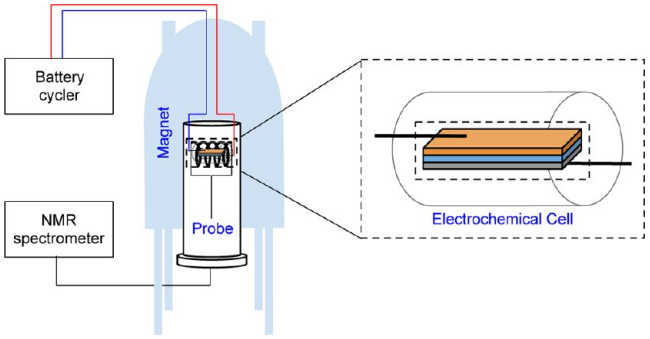


Electrochemical cells, in the form of batteries (or supercapacitors) and fuel cells, are efficient devices for energy storage and conversion. These devices show considerable promise for use in portable and static devices to power electronics and various modes of transport and to produce and store electricity both locally and on the grid. For example, high power and energy density lithium-ion batteries are being developed for use in hybrid electric vehicles where they improve the efficiency of fuel use and help to reduce greenhouse gas emissions. To gain insight into the chemical reactions involving the multiple components (electrodes, electrolytes, interfaces) in the electrochemical cells and to determine how cells operate and how they fail, researchers ideally should employ techniques that allow real-time characterization of the behavior of the cells under operating conditions. This Account reviews the recent use of *in situ* solid-state NMR spectroscopy, a technique that probes local structure and dynamics, to study these devices.

*In situ* NMR studies of lithium-ion batteries are performed on the entire battery, by using a coin cell design, a flat sealed plastic bag, or a cylindrical cell. The battery is placed inside the NMR coil, leads are connected to a potentiostat, and the NMR spectra are recorded as a function of state of charge. $^{7}$Li is used for many of these experiments because of its high sensitivity, straightforward spectral interpretation, and relevance to these devices. For example, $^{7}$Li spectroscopy was used to detect intermediates formed during electrochemical cycling such as $Li_xC$ and $Li_ySi_z$ species in batteries with carbon and silicon anodes, respectively. It was also used to observe and quantify the formation and growth of metallic lithium microstructures, which can cause short circuits and battery failure. This approach can be utilized to identify conditions that promote dendrite formation and whether different electrolytes and additives can help prevent dendrite formation. The *in situ* method was also applied to monitor (by $^{11}$B NMR) electrochemical double-layer formation in supercapacitors in real time. Though this method is useful, it comes with challenges. The separation of the contributions from the different cell components in the NMR spectra is not trivial because of overlapping resonances. In addition, orientation-dependent NMR interactions, including the spatial- and orientation-dependent bulk magnetic susceptibility (BMS) effects, can lead to resonance broadening. Efforts to understand and mitigate these BMS effects are discussed in this Account.

The *in situ* NMR investigation of fuel cells initially focused on the surface electrochemistry at the electrodes and the electrochemical oxidation of methanol and CO to $CO_2$ on the Pt cathode. On the basis of the $^{13}$C and $^{195}$Pt NMR spectra of the adsorbates and electrodes, CO adsorbed on Pt and other reaction intermediates and complete oxidation products were detected and their mode of binding to the electrodes investigated. Appropriate design and engineering of the NMR hardware has allowed researchers to integrate intact direct methanol fuel cells into NMR probes. Chemical transformations of the circulating methanol could be followed and reaction intermediates could be detected in real time by either $^{2}$H or $^{13}$C NMR spectroscopy. By use of the *in situ* NMR approach, factors that control fuel cell performance, such as methanol cross over and catalyst performance, were identified.



Published on the Web 06/21/2013 www.pubs.acs.org/accounts
10.1021/ar400022u 

## 1. Introduction

Concerns about finite energy resources, together with the need to decrease greenhouse gas emissions, have provided considerable incentive to increase usage of renewable energy and to increase the efficiency of devices that produce greenhouse gases such as carbon dioxide. The electrification of transportation (via, for example, the use of hybrid and all-electric vehicles) forms part of this strategy, decreasing use and diversifying the type of fuels that can be used (since multiple fuels can be used to produce the electricity). The increased use of intermittent renewable energy sources on the electric grid is not without challenges and more efficient ways to store and convert electrical energy are required. Fuel cells, batteries, and supercapacitors represent some of the most appropriate technologies for this, particularly for small-scale operations or load-leveling and frequency regulation. For example, lithium-ion batteries (LIBs) have the highest energy densities among the currently available chemical energy storage technologies, with ever-improving power capabilities; they have at least in part enabled the portable technology revolution. LIBs, however, currently fall short of some of the goals for larger end use applications, energy density, safety, and cost all being concerns. Electrical double layer capacitors (EDLCs) or supercapacitors represent another type of energy storage device that find potential uses in the above applications, due to their fast rate of discharge and charge and their essentially unlimited cycle life.[1] Unlike a battery, which uses a redox reaction to store energy, energy is stored in an EDLC via the formation of an electric double layer at the interface between a solid electrode (often a porous carbon electrode) and a liquid electrolyte. Fuel cells (FCs) use an external fuel such as hydrogen, hydrocarbons, or alcohols as the source of chemical energy to produce electrical energy by electrochemical reactions with an oxidant (typically oxygen). Some of the most widely recognized advantages of FCs are their high efficiency, high power density, practically zero waste, and ease by which they can be stacked together to provide devices ranging in size from small portable equipment to large scale power generation.[2]

Fundamental research and development are needed to enable technological breakthroughs and increase market penetration of batteries, supercapacitors, and fuel cells.[3] NMR spectroscopy has played an important role in increasing our understanding of the structure and dynamics of the different components in these devices, including the electrodes, separators, and liquid and solid electrolytes, due to its chemical specificity, its ability to detect dynamical processes that occur over a wide time scale, and its applicability to both crystalline and amorphous materials.

Given the enormity of the field, we concentrate here on the more recent *in situ* NMR investigations, where the systems are investigated during electrochemical cycling. We do not review *ex situ* NMR analysis[4−6] and magnetic resonance imaging (MRI) in fuel cells[7] and batteries,[8] which are all active fields of research. Although the *in situ* approach, to date, does not benefit from the high resolution afforded by magic angle spinning (MAS), there are various magnetic interactions that can be used to probe changes in local environment in electrochemical cells. Changes and formation of phases are often associated with changes in the electronic environment surrounding the nuclei. Several interactions can be used to gauge the electronic environment, namely, the chemical shift, the Knight shift for metals, the Fermi contact shift in the presence of paramagnetic centers, and the quadrupolar interaction. The latter is particularly relevant for LIBs since both $^{7}$Li ($I$ = 3/2, 93% abundance) and $^{6}$Li ($I$ = 1, 7% abundance) are quadrupolar nuclei.

## 2. Li-Ion Batteries and Supercapacitors

*In situ* NMR investigations of batteries allow the different components to be investigated on the same battery at different states of charge. Transient states and the dynamic processes taking place in real time can be studied. In this approach, a whole cell is assembled and mounted into the NMR probe. The cell is then connected to a battery cycler and the spectra are recorded during electrochemical cycling. Early work (on carbonaceous anodes) made use of a toroid cell. In the first steps toward real-time NMR measurements, the increased capacity observed in various synthetic carbons was investigated.[9] A coin cell design was employed with the electrode material directly mounted on the conductor of the NMR circuit for optimal sensitivity and placed in a toroidal cavity detector (TCD).[10] To avoid complications in spectral analysis, the lithium metal and separator were extracted from the cell making the experiment an *ex situ* NMR measurement. A step forward toward *in situ* acquisition was made using a design based on a coin-cell type battery (Figure 1a).[11] The cell is composed of a copper disk that acts as both a current collector in the battery and the NMR detector. The working electrode is then pressed onto the copper disk followed by the separator and the lithium metal counter electrode. The assembly is held together by brass screws on top of a piston that applies uniform pressure to the stacked components of the cell and is placed in a cylindrical metallic container

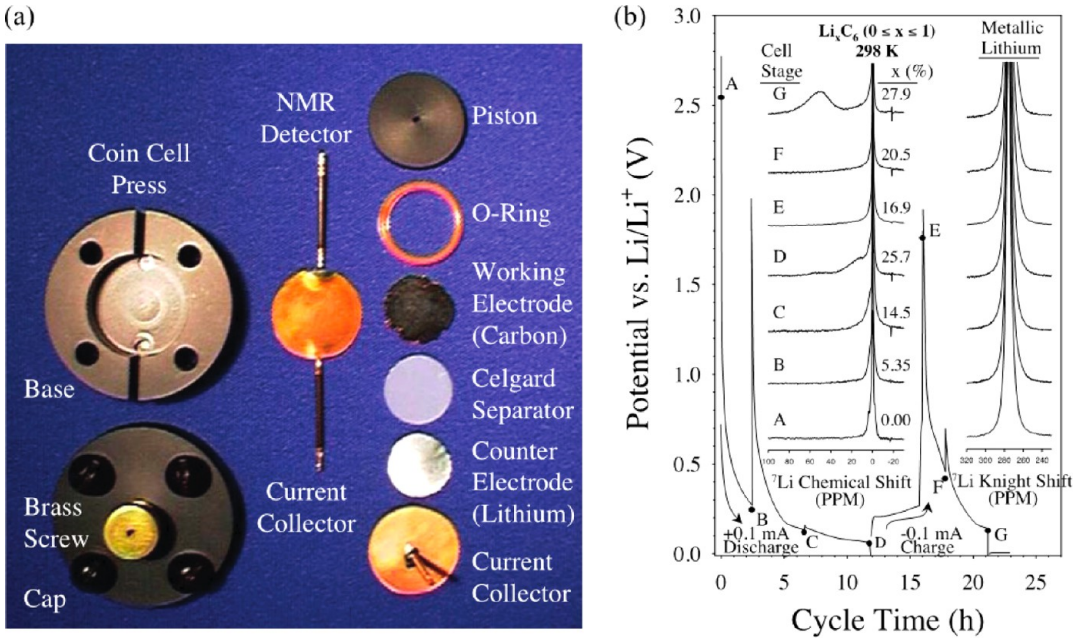


**FIGURE 1.** (a) The compression coin cell battery. (b) Voltage profile and $^7$Li NMR spectra for one cycle of Li/composite carbon cell. Spectra were recorded for points A−G and separated for the metal region (right inset) and reacted lithium (left inset). Figure adapted from ref 11. Copyright 2001 Institute of Physics Publishing.

(the toroid). This setup allows alternating *in situ* electrochemical and NMR measurements to be performed by connecting and disconnecting a potentiostat to the rods attached to the current collectors. The radio frequency (RF) current applied to the circuit creates an inhomogeneous RF magnetic field across the layers stacked on top of the detector. Thus, composite pulse sequences were employed to achieve uniform excitation of the nuclear spins in the different regions of the cell. (The inhomogeneity in signal excitation/detection was also employed to image the various components). Lithium intercalation in a blend of spherical and flaky graphitic carbon particles was investigated by recording static $^7$Li spectra at different states of charge (Figure 1b). The study made use of *ex situ* NMR studies of lithium insertion into graphite, which showed a progressive Knight shift of the $^7$Li resonance to higher frequency with increasing Li intercalation between the graphitic sheets[12] and a change in the quadrupole line shape due to the change in the local electric field gradient induced by the surrounding hexagonal carbon units.[13] Resonances are, for example, observed due to dense stage I or II compounds ($LiC_6$ and $LiC_{12}$; ∼50 ppm) at the end of discharge.

The separation of the battery components from the NMR hardware enabled the first *in situ* continuous NMR studies.[14−16] The cell design was based on the plastic batteries developed by Bellcore,[17] where the two electrodes (here carbon and lithium) are attached to copper mesh current collectors, thermally laminated to the opposite sides of the separator and packaged and sealed in an aluminum-coated plastic bag (Figure 2a). The whole flexible cell can now fit into a standard 10 mm solenoid NMR coil. The *in situ* NMR spectra of a cell containing disordered carbon (Figure 2b) show an intense $^7$Li $LiPF_6$ electrolyte peak at −2 ppm and a metal (Li) peak at 263 ppm (not shown). As the cycling commences, a new peak appears, which shifts to higher frequency with discharge (lithium insertion). The peak was assigned to quasi-metallic lithium located in the bulk of the carbon fiber where there are fewer graphenic layers and they are more disordered. This environment is responsible for the large reversible capacity of these carbons. A fourth peak at about 18 ppm was assigned to lithium in more ordered graphitic regions. Lithium insertion into natural graphite electrodes was then compared with results for carbon composite electrodes comprising graphene-coated pyrolized carbon cloths.[18] The *in situ* measurements of graphite provided clear assignments of the NMR shifts and quadrupolar coupling constants for the different lithiated graphite phases, which were quite distinct from the two featureless resonances (intercalated and quasi-metallic lithium) of the carbon composite electrode.

The methodology was extended to investigate alloying of lithium in silicon anodes.[20] Silicon is an attractive alternative to carbon, potentially offering a 10-fold increase in both volumetric and gravimetric capacity. A downside is a

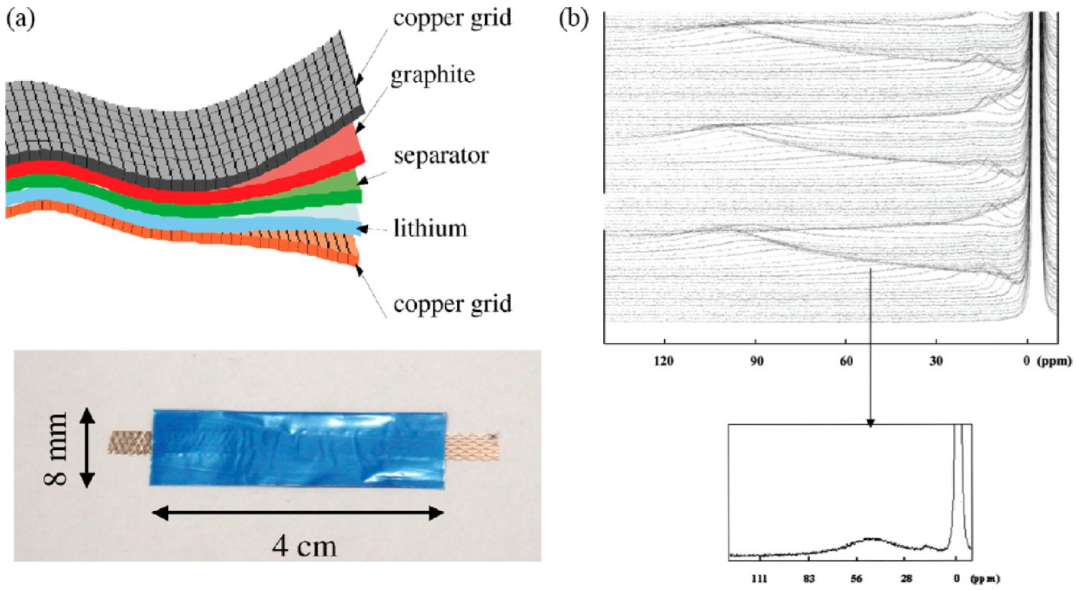


**FIGURE 2.** (a) Schematic representation of the Bellcore plastic bag cell. Reprinted with permission from ref 19. Copyright 2007 Elsevier. (b) $^{7}$Li NMR spectra acquired during insertion/deinsertion in carbon fabric. Inset shows detail of one spectrum showing the two peaks corresponding to inserted lithium. Reprinted with permission from ref 15. Copyright 2003 The Electrochemical Society.

volume expansion of 300%, often resulting in a loss of particle connectivity and capacity fade. As lithium insertion commences, amorphous phases are formed thus limiting the applicability of diffraction techniques to follow structural changes. $^{7}$Li NMR spectra obtained during lithium insertion are shown in Figure 3, along with the cell design. The four resonances in the region 0−8 ppm observed in the initial spectrum are due to lithium in the electrolyte, the solid electrolyte interface (SEI) layer, and a $Li_xC$ phase. During cell discharge three distinct lithium environments can be identified: the resonance that shifts from 18 to 14 ppm is assigned to lithium nearby small silicon clusters; the sharp intense resonance at 4.5 ppm is due to lithium nearby isolated silicon ions with some contribution from SEI components; finally the resonance at −10 ppm, which appears at deep discharge, is assigned to a crystalline phase with stoichiometry close to $Li_{15}Si_4$. Comparison with the *ex situ* NMR data indicates that this crystalline phase is metastable and reacts with the electrolyte via a "self-discharge" process. This process can be slowed by the addition of binders such as carboxymethylcellulose.

Lithium metal represents the ultimate anode material. However, its use is considered hazardous due to the formation of lithium microstructures (mossy or dendritic lithium deposits on the surface of the bulk lithium metal) upon extended cycling.[3] These microstructures can detach from the anode and migrate to the cathode side, causing a short circuit that can result in a rapid heat release that can ignite the flammable organic electrolyte. *In situ* NMR can be used to identify conditions in which these microstructures are formed and monitor their evolution in a quantitative

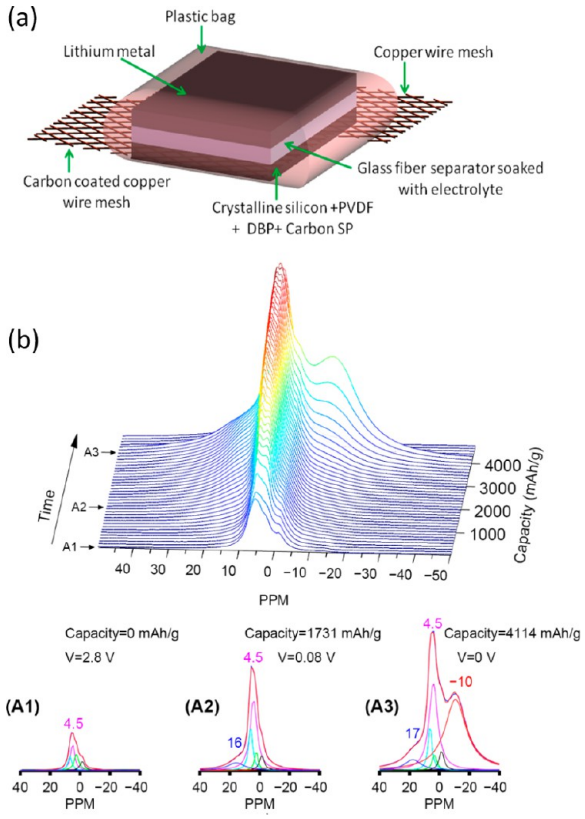


**FIGURE 3.** (a) Schematic of the flexible plastic battery. (b) Stacked plots of *in situ* $^{7}$Li NMR spectra of a crystalline Si vs Li/Li$^{+}$ battery. Representative deconvoluted $^{7}$Li spectra at various discharge capacities (A1, A2, A3) shown below the *in situ* experiments. Reprinted with permission from ref 20. Copyright 2009 American Chemical Society.

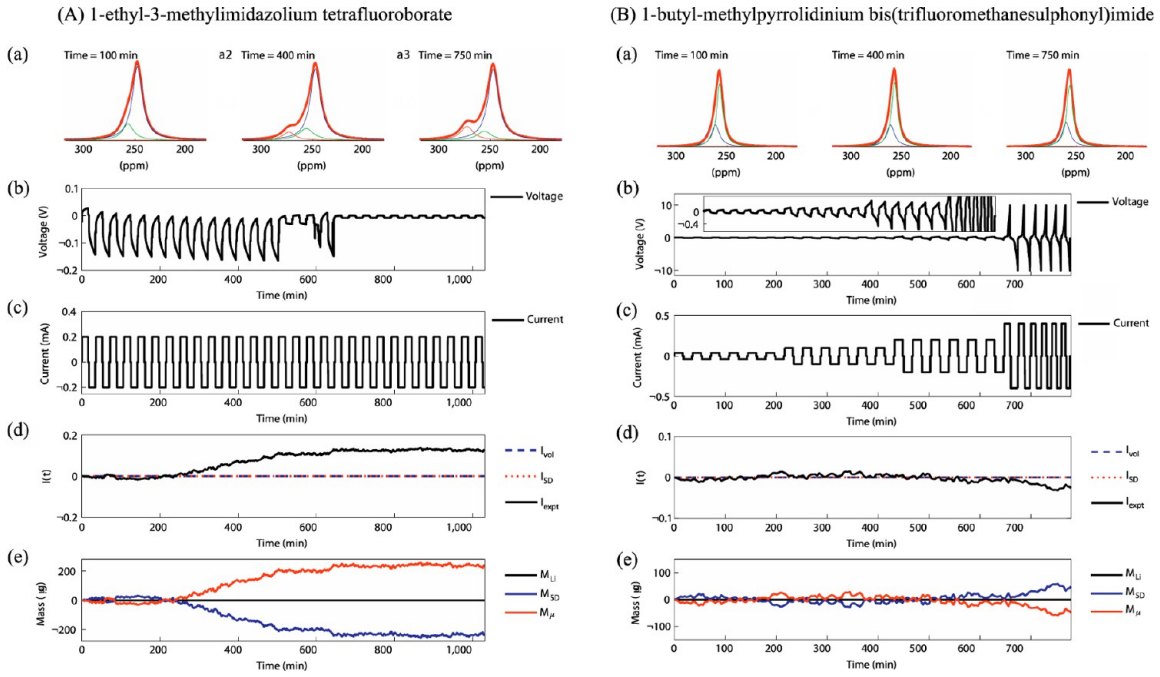


**FIGURE 4.** Effect of multiple cycles on the $^7$Li NMR spectra of a metallic lithium symmetric cell containing $C_2$ min $BF_4$ (A) or $C_4$ mpyr TFSI (B) ionic liquid electrolytes. (a) Deconvoluted $^7$Li NMR resonances at three different times. (b, c) Measured voltage and applied current during the electrochemical cycling. (d) Experimental NMR signal intensity, $I_{expt}$, and calculated intensities under the assumptions that there is no skin depth issues ($I_{vol}$) and that all lithium is smoothly deposited ($I_{SD}$). (e) $I_{expt}$ was used to calculate the mass of the deposited lithium in the case of microstructures ($M_{\mu}$), smooth deposition of lithium ($M_{SD}$), and the total Li mass ($M_{Li}$). Reprinted with permission from ref 21. Copyright 2010 Macmillan Publishers Limited.

manner, this approach making use of the limited penetration depth of the RF field into the bulk lithium metal.[21] As a result, only the surface and subsurface regions (up to approximately 13 $\mu$m) of lithium metal are detected, while lithium nuclei in the thin microstructures can be fully excited and detected (since they are <5 $\mu$m in diameter). This approach was utilized to monitor microstructure formation in two ionic liquid electrolytes (1-ethyl-3-methylimidazolium tetrafluoroborate ($C_2$min $BF_4$) and 1-butyl-methylpyrrolidinium bis(trifluoromethanesulfonyl)imide ($C_4$mpyr TFSI)) differing in their ability to suppress dendrite formation. The results performed on symmetric bag cells (with lithium metal on both electrodes) containing the $C_2$min $BF_4$ electrolyte (Figure 4A) show the formation of microstructures on cycling (Figure 4Aa) in the form of a growing peak at 270 ppm. The unchanged resonance at 250 ppm corresponds to lithium at the surface of the bulk lithium. Models based on either no skin-depth issues ($I_{vol}$) or assuming that the lithium is smoothly deposited on the surface of the lithium metal ($I_{SD}$) do not fit the signal intensity ($I_{exp}$) (Figure 4Ad). By taking into account the skin depth issue, the mass of the microstructures that are formed can be calculated (figure 4Ae). When the $C_4$mpyr TFSI electrolyte is used, no growth of the Li microstructures is observed (Figure 4B) after cycling for more than 12 h, even when high currents are used; the paper also explored the role of stable SEI formation in microstructure formation. This paper was the first to exploit the magnetic susceptibility (BMS) effects that occur in these systems to separate the signal arising from lithium in the microstructures from that of the bulk metal.

Bulk magnetic susceptibility (BMS) effects play a significant role in all static *in situ* NMR measurements.[22] While those in diamagnetic materials are typically small, they should be taken into account for a full and accurate assignment of the spectra. When metallic and paramagnetic electrodes are introduced into the cell, these effects are increased due to the presence of delocalized or unpaired electrons, respectively. BMS effects arise due to interactions at the particle level (when the sample is heterogeneous and composed of several components), as well as macroscopic phenomena that depend on the overall shape of the sample. The effect on the $^7$Li shift of lithium metal is demonstrated in Figure 5a, where the resonance shifts about 30 ppm as the lithium metal strip is rotated in the NMR coil. The lithium metal (and other conductive components such as graphite) will also affect the shifts and broadening of the other (e.g., the electrolyte) components in the cell. For paramagnetic materials these effects become even more significant, and

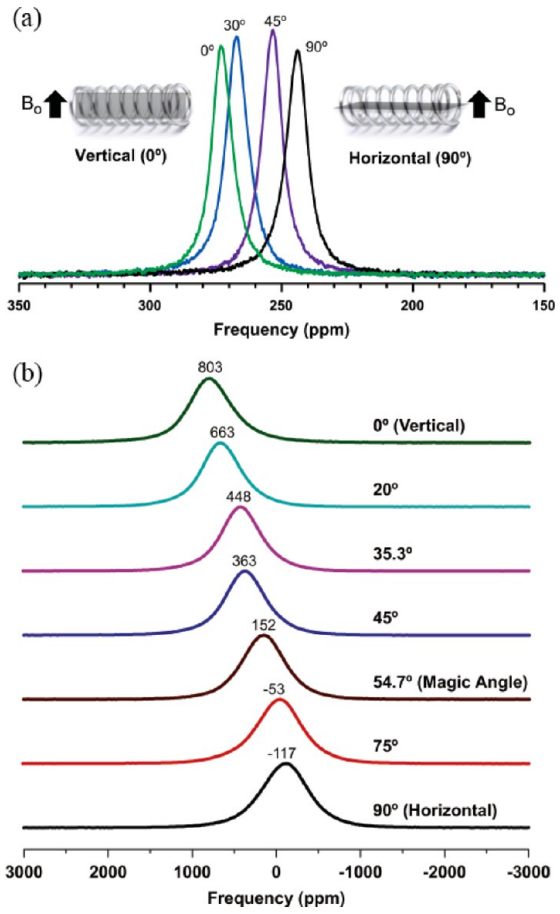


**FIGURE 5.** (a) $^{7}$Li bulk magnetic susceptibility effects for lithium metal strips, with their short axes oriented at the specified angles with respect to $B_0$. (b) $^{7}$Li static spectra of $Li_{1.08}Mn_{1.92}O_4$ film at different orientations with respect to $B_0$. Reprinted with permission from ref 22. Copyright 2012 Elsevier.

this coupled with the large line broadening associated with the electron−nuclear dipolar interactions, render *in situ* NMR investigations of, for example, transition metal oxides extremely challenging. Nevertheless they can be accounted for as is demonstrated in Figure 5b where the $^{7}$Li static spectra acquired from a manganese spinel ($Li_{1.08}Mn_{1.92}O_4$) electrode film is plotted as a function of the film's orientation with respect to the magnetic field. A shift range of 900 ppm is covered when the film is rotated by 90° due to the BMS.[23]

Susceptibility effects were exploited in the *in situ* NMR investigation of EDLCs, to gain a deeper understanding of the mechanisms of double layer formation and factors affecting the capacitance.[24] The plastic bag cell design was modified such that the two electrodes were sheared along the cell's long axis so as to separate the resonances from the two electrodes, only one electrode being placed in the NMR coil (Figure 6a). $^{11}$B NMR spectra acquired from a cell composed of porous YP-17 carbon electrodes and

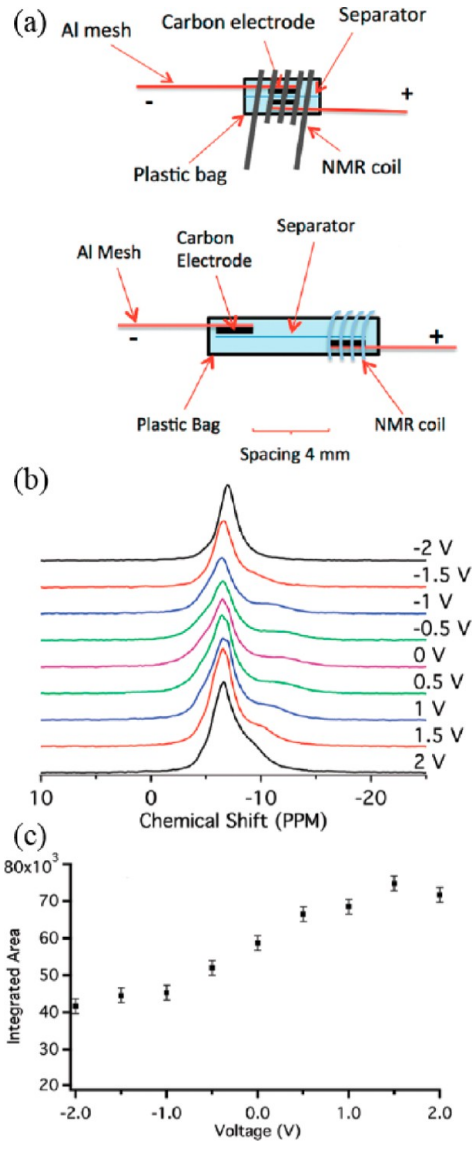


**FIGURE 6.** (a) EDLC cell designs for *in situ* NMR studies: standard (top) and modified "long" cell with two separate electrodes (bottom). (b) $^{11}$B NMR spectra of the electrode charged from −2 to 2 V (top) and (c) the integrated areas of the spectra as a function of the applied voltage. Reprinted with permission from ref 24. Copyright 2011 American Chemical Society.

$BF_4^-$ tetraethylammonium salt in acetonitrile electrolyte (Figure 6b) contained three major resonances, which were assigned to $BF_4^-$ ions in the double layers near the carbon surfaces (most negative shifts), weakly bound ions that are shifted downfield, and a narrow peak due to free ions in the electrolyte. This assignment was based on titration experiments in which a controlled amount of electrolyte was added to the electrode while monitoring the growth of the three environments and on separate relaxation measurements. As expected, the total integrated signal intensity decreases as the voltage is lowered to −2 V, consistent with removal of

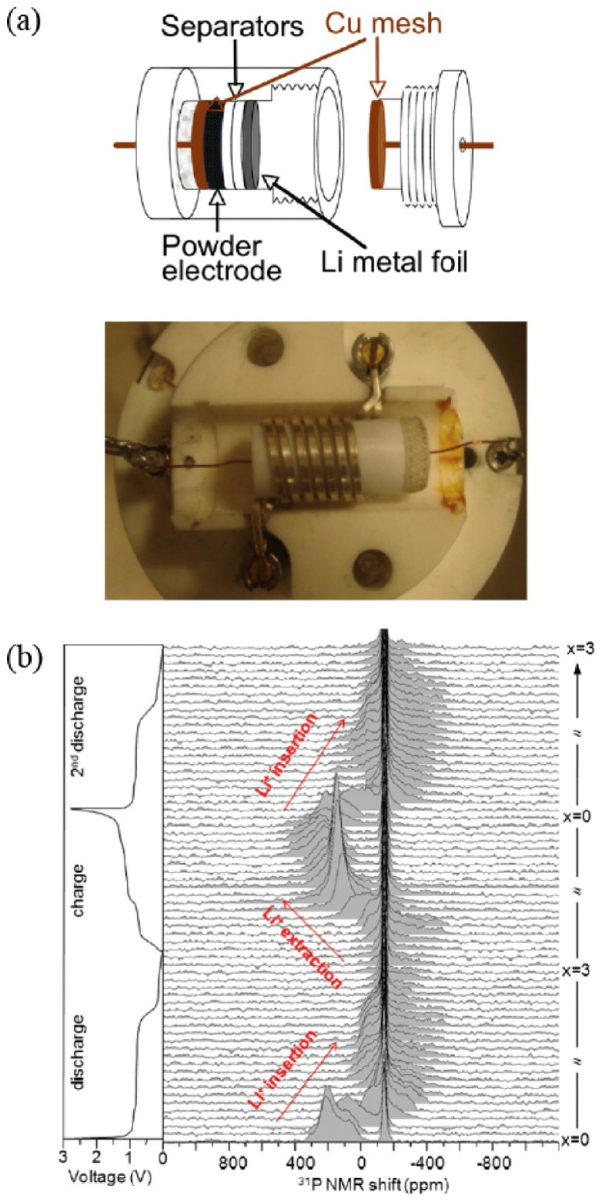


**FIGURE 7.** (a) Schematic drawing of the cylindrical cell design for *in situ* NMR experiments (top) and a top view of the NMR probe with the cylindrical cell inside a 10 mm solenoid (bottom). (b) Stack plot of selected *in situ* $^{31}$P NMR spectra recorded during the first and second half cycle of a $Cu_3P$ electrode vs Li. The vertical axis represents molar fraction ($x$) of Li ions. Reprinted with permission from ref 25. Copyright 2011 Elsevier.

the $BF_4^-$ ions from the electrode and diffusion of the ions to the side of the cell outside of the NMR coil (Figure 6c). The strongest influence of the voltage is on the $BF_4^-$ resonance ascribed to the ions near the carbon, its spin-relaxation time decreasing at positive potentials, and its intensity increasing as more ions enter the pores on charging.

While the plastic bag cell is used in most *in situ* measurements performed to date due to its clear benefits such as low metal content, ease of assembly, and flexibility, it suffers from limited filling factor. In addition, care must be taken to prevent electrolyte leakage, air and moisture contamination, and loss of contacts between the electrodes (due to the lack of external pressure). To overcome these difficulties but still benefit from the use of standard NMR probes, Poli et al.[25] designed a new cell comprising a robust cylindrical plastic (polypropylene) housing, which is easy to assemble and can be filled with powders, allowing the amount of active component under investigation to be increased (Figure 7a). The cell housing is open on one side and equipped with a screw-like cap for tight sealing. Copper wire current collectors are inserted through the bottom of the cell and its cap. The cell performed well during the initial cycles, but capacity fading was then observed possibly due to loss of pressure. $^{31}$P *in situ* NMR measurements were carried out on the anode material, $Cu_3P$ (Figure 7b). The pristine $Cu_3P$ signal is observed at 160 ppm, and the electrolyte salt, $LiPF_6$, is observed at −143.6 ppm. Upon discharge, a new $^{31}$P environment is formed at −270 ppm, corresponding to $Li_3P$ disordered phase, which is not observed by diffraction techniques. The cylindrical shape of this new cell may lend itself to MAS NMR techniques, if an approach that allows for stable spinning could be found.

## 3. Fuel Cells

*In situ* NMR studies on fuel cells (FCs) have focused on probing the chemical reactions at the electrodes and the fate of fuels such as methanol during FC operation. Reaction intermediates of fuel oxidation can be observed, pathways to cell degradation identified, and catalyst efficiency investigated under multiple operating conditions. Pioneering work investigated only one electrode under potential control,[26] while more recent work[27] has focused on using a more technically challenging setup involving placing an actual FC inside a custom-built NMR probe and allowing the fuel and oxidant to flow in and out of the cell.

Following the preliminary investigation of the electrooxidation of $^{13}CH_3OH$ on Pt electrode by *ex situ* surface NMR electrochemistry,[4] the first *in situ* NMR electrochemical cell (Figure 8a)[26,28] involved a powdered Pt-black working electrode, conditioned for adsorption with $^{13}CH_3OH$ in aqueous $H_2SO_4$ under potentiostat control outside the cell. The Pt working electrode and solution were transferred into the NMR cell comprising a 10 mm NMR tube containing the electrodes, the Pt electrode being placed inside the NMR coil and connected to an external potentiostat with a platinum wire. The complete stepwise oxidation of $^{13}CH_3OH$ to form $^{13}CO$ and then $^{13}CO_2$ on the Pt black electrode could be

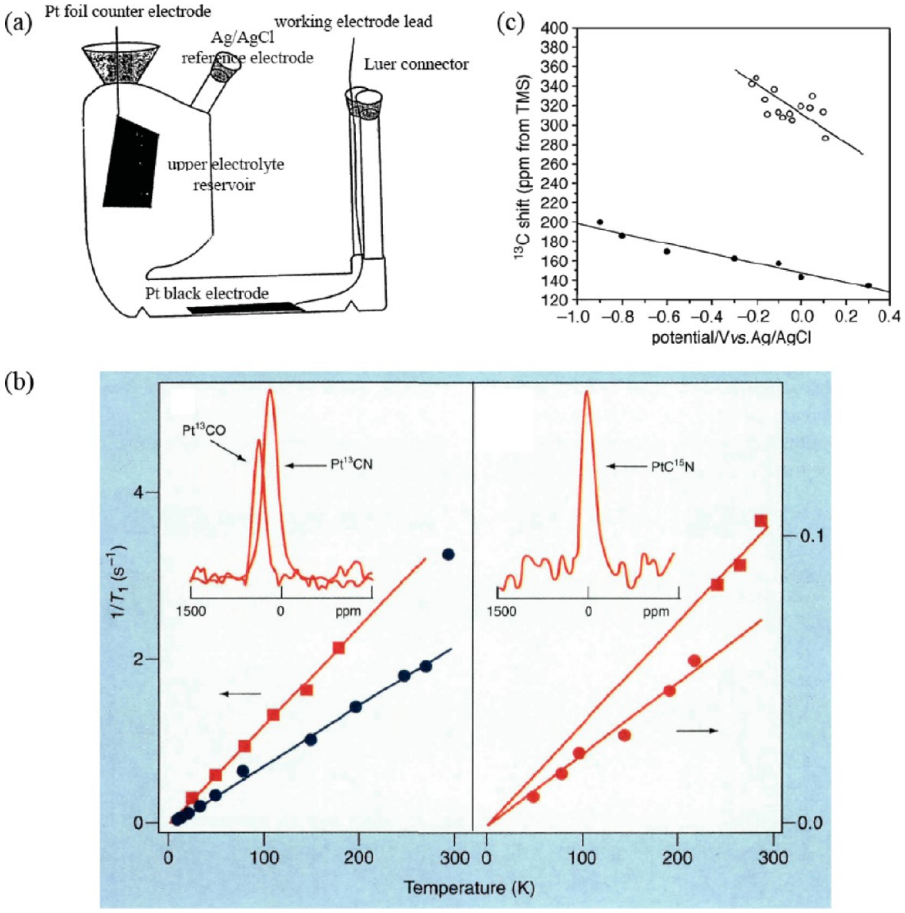


**FIGURE 8.** (a) *In situ* electrochemical NMR cell. Reprinted with permission from ref 29. Copyright 1997 Royal Society of Chemistry. (b) $^{13}$C and $^{15}$N NMR surface spectra and corresponding Korringa relationships of Pt$^{13}$CO(ads) (■), Pt$^{13}$CN(ads) (●) and PtC$^{15}$N(ads) (●, ■) obtained by electro-oxidation of $^{13}$C-labeled $^{13}CH_3OH$ in $H_2SO_4$, adsorption of $^{13}$C-labeled Na$^{13}$CN, and $^{15}$N-labeled NaC$^{15}$N in $Na_2SO_4$, respectively, and their corresponding Korringa relationships. Reprinted with permission from ref 30. Copyright 1998 American Chemical Society. (c) $^{13}$C chemical shift vs potential for Pt$^{13}$CN(ads) (●) and Pt$^{13}$CO(ads) (○). Reprinted with permission from ref 29. Copyright 1997 Royal Society of Chemistry.

monitored by $^{13}$C NMR, while varying the electrode potential. Pt$^{13}$CO(ads) was first observed as a broad and downfield resonance,[4] with a Knight shift of ~200 ppm, the broadening largely arising from the $^{13}$C chemical shift anisotropy (CSA) and an anisotropic contribution to the Knight shift. As the electrode potential is increased, line narrowing was observed and ascribed to the oxidation of adsorbed $^{13}$CO, which is stripped off the surface as $^{13}CO_2$ gas dissolved in the solution (Figure 9b).[26,28]

The sensitivity of this NMR electrochemical prototype cell was then improved and the cell modified to allow conditioning of the Pt electrode directly inside the electrochemical cell (Figure 9a).[29] $^{13}$C NMR spectra of Pt$^{13}$CO and Pt$^{13}$CN (obtained by electro-oxidation of $^{13}CH_3OH$ and Na$^{13}$CN, respectively) were obtained in less than 4 h with very good signal-to-noise ratios (Figure 9b).[29,30] Both samples have similar line shapes, dominated by $^{13}$C CSA, Knight shift anisotropies, and broadening from magnetic field gradients from the Pt demagnetizing fields. Pt$^{13}$CO resonates at a shift that is ~170 ppm from CO in the gas phase (~160 ppm), due to a Knight shift caused by the interaction with the metallic Pt. The $^{13}$C spin−lattice relaxation times ($T_1$s) of Pt$^{13}$CO have been determined as a function of temperature ($T$),[29,31] and the $T_1$ was found to be inversely proportional to $T$, demonstrating that the $T_1$ relaxation mechanism is driven by conductive electron spins satisfying the Korringa equation:[32]

$$T_1T = \left(\frac{\hbar}{K^2 4\pi k_B}\right)\left(\frac{\gamma_e}{\gamma_n}\right)^2 B$$

where $\gamma_e$ and $\gamma_n$ are the gyromagnetic ratios of the electron and the nucleus (rad·s$^{-1}$·T$^{-1}$), $K$ is the knight shift (ppm), $\hbar$ is the Plank constant, $k_B$ is the Boltzmann constant, and $B$ is a constant close to unity.[32] This further confirms the binding of $^{13}$CO to metallic Pt, the small Korriga product ($T_1T \approx 82$ sK) being indicative of strong metal. The $^{13}$C resonance of Pt$^{13}$CN is observed at ~170 ppm indicating a weaker

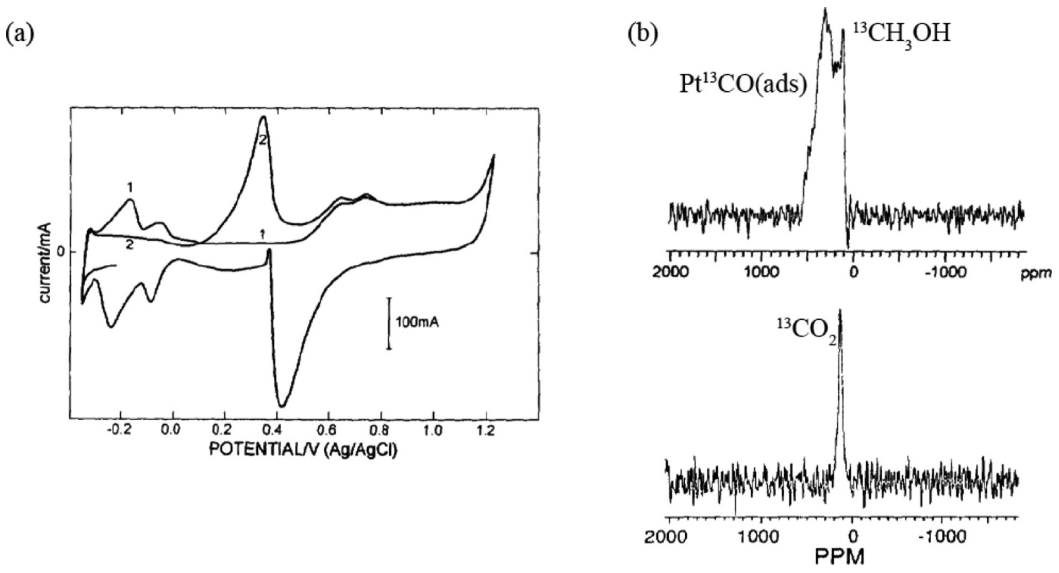


**FIGURE 9.** (a) Voltammogram obtained in clean $H_2SO_4$ after $^{13}CH_3OH$ adsorption at −0.2 V for 36 h. (b) $^{13}C$ NMR spectrum of $^{13}CO$ adsorbed into Pt(ads) obtained from decomposition of $^{13}CH_3OH$ onto powdered Pt black electrode at a potential of −0.2 V (top) and +0.4 V (bottom). Reprinted with permission from ref 28. Copyright 1993 Elsevier.

overlap between the carbon orbitals and the Pt conduction band. However, up to 273 K, the $Pt^{13}CN$ $T_1$ values still obey a Korringa relationship with $T_1T \approx 135$ sK, indicating a degree of metallicity. $^{15}N$ spectra of $PtC^{15}N$ confirmed this analysis. The strong electrostatic field effects at the electrode/electrolyte interface were also investigated, the $^{13}C$ resonances becoming more shielded as the electrode potential is increased (Figure 8c).

Using a different design, electrocatalytic oxidation of CO was conducted where layers of carbon-supported Pt electrode were placed within the NMR coil. $^{13}C$ NMR spectra were obtained, and the typical $^{13}C$ line shape of $Pt^{13}CO$ observed.[33] A linear correlation between the $^{13}C$ NMR signal $Pt^{13}CO$ as a function of CO surface coverage and the number of surface CO obtained by couloumetry was obtained, demonstrating that the approach could be used quantitatively to investigate the mechanism of CO electrocatalytic oxidation and the reaction pathways.[34] Three different states of adsorbed CO onto Pt and their oxidation reaction pathways were proposed where CO is linearly adsorbed (major species), bridged, or partially reduced ($CHO_{ads}$), the relative populations depending on the electrochemical potential of adsorption but not on the CO coverage.

Adsorbate−metal interactions were also investigated by *ex situ* $^{195}Pt$ NMR using a frequency sweep approach.[35] Similar to platinum-supported heterogeneous catalysts,[36] the resonances from platinum nuclei on the surfaces are shifted to low field (at 1.089 G/kHz corresponding to $PtO_2$)[36,37] as compared with bulk platinum (at 1.138 G/kHz)[38] in line with an increase of the Knight shift. The electrochemistry and $^{195}Pt$ NMR spectra of these electrodes were found to be particle size dependent, and bulk vs surface signals were readily separated.[39]

Direct detection of the methanol and methanol electro-oxidation intermediates traveling through a direct methanol fuel cell (DMFC) was obtained by *ex situ* NMR spectroscopy.[40] A membrane electrode assembly (MEA) fabricated with a triple layer polymer electrolyte membrane (PEM) containing a PEM electrolyte layer sandwiched between a PtRu/C anode and a Pt/C cathode was operated as a DMFC with an aqueous solution of $^{13}CH_3OH$ as the fuel. The cell was then disassembled, and the central PEM electrolyte layer components were identified by $^{13}C$ MAS NMR, the cross over of $CH_3OH$ from the anode to the cathode being clearly observed. Reaction intermediates of methanol oxidation were also observed. Comparison between a MAE with Pt/C vs PtRu/C at the anode revealed the presence of a higher concentration of formic acid in line with lower catalytic activity of the former for methanol electro-oxidation.[41]

Successful integration of the DMFCs discussed above into a home-built NMR probe[42] allowed the oxidation of $CD_3OH$ in DMFCs to be followed by *in situ* $^2H$ NMR.[43] The probe used a TCD[10] as the NMR coil, its sensitivity and resolution being sufficient to allow time-resolved NMR experiments to be performed without disassembly of the electrochemical cell.[40] The central conductor of the toroid was also used as the anode current collector while the MEA was located inside the outer conductor, and the cathode was connected to the

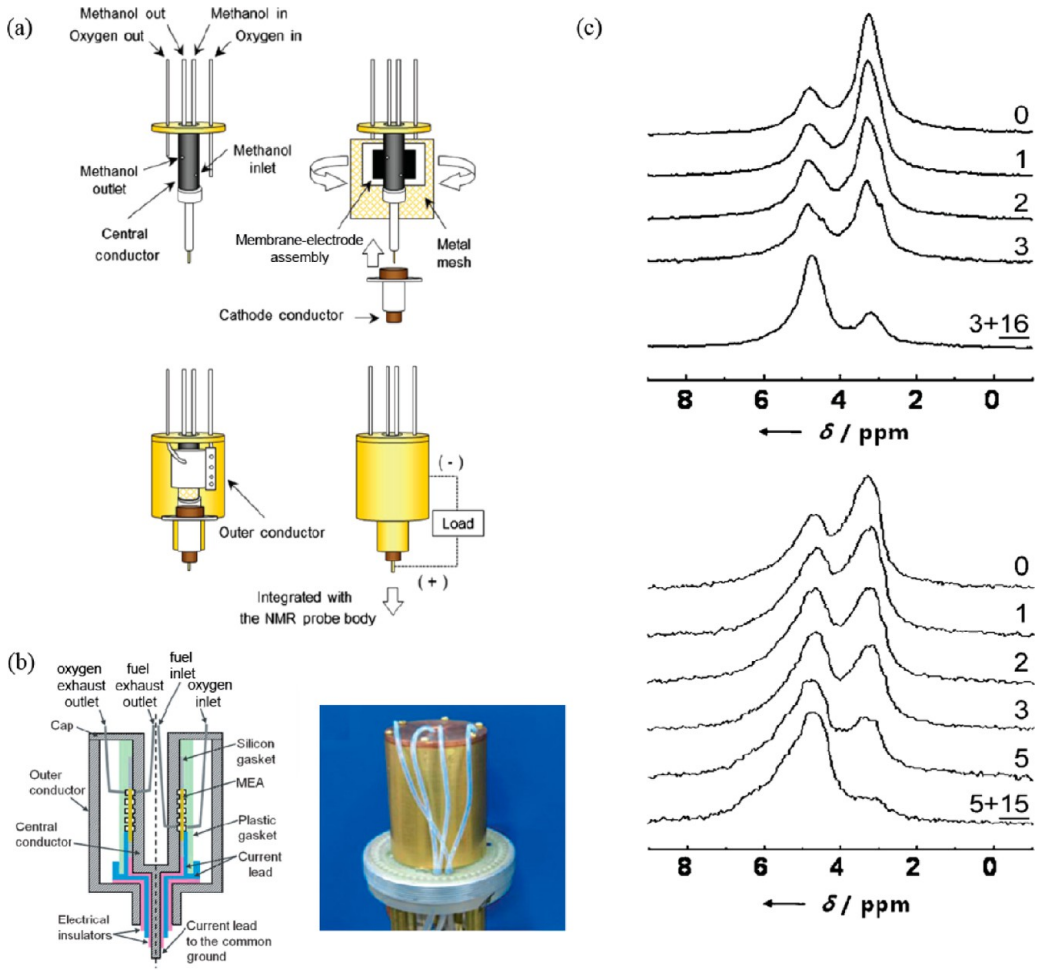


**FIGURE 10.** (a) Schematic representation of an integrated DMFC inside a TCD. (b) (left) Sliced viewed of the DMFC. (right) Photograph of the probe after assembly. (c) $^2$H NMR spectra of $CD_3OH$ during FC operation with PtRu/C (top) and Pt/C (bottom) anode catalysts. Cumulative fuel-cell operation hours are labeled. Underlined numbers denote hours in open-circuit mode. Reprinted with permission from ref 43. Copyright 2012 Wiley-VCH Verlag GmbH & Co. KGaA.

potentiostat (Figure 10b). As described above for the early studies of batteries, the current collectors were then disconnected electrically during the RF pulses to avoid interference or undesirable noise. Complete electro-oxidation of aqueous $CD_3OH$ proceeds through

$$CD_3OH + H_2O \rightarrow CO_2 + 3D^+ + 3H^+ + 6e^-$$

where $D^+$ quickly reacts with OHs (from methanol, $H_2O$, or reaction intermediates) to produce adsorbed OD species. Figure 10d shows the $^2$H spectra of the two different DMFCs with different anode catalysts where both the fuel ($CD_3OH$) and the adsorbed OD species are observed at 3.3 and 4.8 ppm, respectively, demonstrating that chemical reactions in DMFCs could be monitored by *in situ* NMR. As methanol oxidation occurs, the ratio of the 3.3 vs 4.8 ppm signals decreased following the consumption of methanol. More importantly, this experimental NMR setup also allowed for rapid testing of different anode catalysts, PtRu/C showing better efficiency and faster methanol oxidation than Pt/C.

## 4. Conclusions

We have described some recent applications of NMR spectroscopy to follow, in real time, the electrochemical processes that occur in batteries, supercapacitors, and fuel cells. These studies, in close concert with relevant *ex situ* NMR studies, show considerable promise in helping to understand how such electrochemical cells function and why they sometimes fail during operation and to, for example, screen materials (anode, cathode and electrolytes) and identify the experimental conditions under which the cells will be more robust. This NMR methodology plays an important role in the development of new and improved electrochemical devices needed to store and convert electricity more

efficiently, an important part of worldwide strategies to reduce $CO_2$ emissions.

*F.B. and M.L. thank the EU Marie Curie actions FP7 for an International Incoming fellowship (F.B.) and an Intra-European fellowship (M.L.). F.B. also thanks Clare Hall, University of Cambridge, for a Research Fellowship. M.L. is an awardee of the Weizmann Institute of Science–national postdoctoral award program for advancing women in science. C.P.G. thanks the EU ERC for an Advanced Fellowship and NECCES, an Energy Frontier Research Center funded by the U.S. DOE (DE-SC0001294), for support of the in situ NMR method development.*

## BIOGRAPHICAL INFORMATION

**Frédéric Blanc** received his Ph.D. in Chemistry from the University of Lyon in 2007 working with Prof. Christophe Copéret and Prof. Lyndon Emsley on solid-state NMR methods to characterize surfaces. He worked with Prof. Clare P. Grey studying proton and ionic conductors by NMR spectroscopy, as a Lavoisier postdoctoral fellow at Stony Brook University and then as Marie Curie research fellow at the University of Cambridge. He recently joined the faculty of the University of Liverpool as a Lecturer in Chemistry.

**Michal Leskes** received her Ph.D. in Chemistry from the Weizmann Institute of Science in 2010 working with Prof. Shimon Vega on methodology development for high-resolution proton solid-state NMR. She is now a Marie Curie research fellow working with Prof. Clare P. Grey on NMR studies of lithium ion batteries.

**Clare P. Grey** is the Geoffrey Moorhouse-Gibson Professor of Chemistry at Cambridge University. She received a B.A. and D.Phil. (1991) in Chemistry from the University of Oxford. After spending two years as a visiting scientist at DuPont in Wilmington, DE (1992–1993), she joined the faculty at Stony Brook University (SBU) as an Assistant (1994), Associate (1997), and then Full Professor (2001). Since moving to Cambridge in 2009, she maintains a part-time position at SBU, where she is the Associate Director of the DOE funded Northeastern Chemical Energy Storage Center. Her research interests include the use of NMR and diffraction methods to investigate materials for energy storage and conversion and in environmental chemistry.

## FOOTNOTES

*To whom correspondence should be addressed. E-mail: cpg27@cam.ac.uk (C.P.G.).
The authors declare no competing financial interest.

## REFERENCES

1 Simon, P.; Gogotsi, Y. Materials for electrochemical capacitors. *Nat. Mater.* **2008**, *7*, 845–854.

2 Wachsman, E. D.; Lee, K. T. Lowering the temperature of solid oxide fuel cells. *Science* **2011**, *334*, 935–939.

3 Tarascon, J.-M.; Armand, M. Issues and challenges facing rechargeable lithium batteries. *Nature* **2001**, *414*, 359–367.

4 Chan, K. W. H.; Wieckowski, A. Probing adsorbates on Pt electrode surfaces by the use of $^{13}C$ spin-echo NMR. Studies of CO generated from methanol electrosorption. *J. Electrochem. Soc.* **1990**, *137*, 367–368.

5 Grey, C. P.; Dupré, N. NMR studies of cathode materials for lithium-ion rechargeable batteries. *Chem. Rev.* **2004**, *104*, 4493–4512.

6 Blanc, F.; Spencer, L.; Goward, G. R. *Quadrupolar NMR of Ionic Conductors, Batteries, and Other Energy-related Materials in Encyclopedia of Magnetic Resonance*; John Wiley: Chichester, 2011; DOI: 10.1002/9780470034590.emrstm1215.

7 Feindel, K. W.; LaRocque, L. P.-A.; Starke, D.; Bergens, S. H.; Wasylishen, R. E. In situ observations of water production and distribution in an operating $H_2/O_2$ PEM fuel cell assembly using $^1H$ NMR microscopy. *J. Am. Chem. Soc.* **2004**, *126*, 11436–11437.

8 Chandrashekar, S.; Trease, N. M.; Chang, H. J.; Du, L.-S.; Grey, C. P.; Jerschow, A. $^7Li$ MRI of Li batteries reveals location of microstructural lithium. *Nat. Mater.* **2012**, *11*, 311–315.

9 Gerald, R. E., II; Klingler, R. J.; Sandí, G.; Johnson, C. S.; Scanlon, L. G.; Rathke, J. W. $^7Li$ NMR study of intercalated lithium in curved carbon lattices. *J. Power Sources* **2000**, *89*, 237–243.

10 Rathke, J. W.; Klingler, R. J.; Gerald, R. E., II; Kramarz, K. W.; Woelk, K. Toroids in NMR spectroscopy. *Prog. Nucl. Magn. Reson. Spectrosc.* **1997**, *30*, 209–253.

11 Gerald, R. E., II; Sanchez, J.; Johnson, C. S.; Klingler, R. J.; Rathke, J. W. In situ nuclear magnetic resonance investigations of lithium ions in carbon electrode materials using a novel detector. *J. Phys.: Condens. Matter* **2001**, *13*, 8269–8285.

12 Dai, Y.; Wang, Y.; Eshkenazi, V.; Peled, E.; Greenbaum, S. G. Lithium-7 nuclear magnetic resonance investigation of lithium insertion in hard carbon. *J. Electrochem. Soc.* **1998**, *145*, 1179–1183.

13 Sandí, G.; Gerald, R. E., II; Scanlon, L. G.; Johnson, C. S.; Klingler, R. J.; Rathke, J. W. Molecular orbital and Li-7 nmr investigation of the influence of curved lattices in lithium intercalated carbon anodes. *J. New Mater. Electrochem. Syst.* **2000**, *3*, 13–19.

14 Letellier, M.; Chevallier, F.; Clinard, C.; Frackowiak, E.; Rouzaud, J. N.; Béguin, F.; Morcrette, M.; Tarascon, J.-M. The first in situ $^7Li$ nuclear magnetic resonance study of lithium insertion in hard-carbon anode materials for Li-ion batteries. *J. Chem. Phys.* **2003**, *118*, 6038–6045.

15 Chevallier, F.; Letellier, M.; Morcrette, M.; Tarascon, J.-M.; Frackowiak, E.; Rouzaud, J.-N.; Béguin, F. In situ $^7Li$-nuclear magnetic resonance observation of reversible lithium insertion into disordered carbons. *Electrochem. Solid-State Lett.* **2003**, *6*, A225–A228.

16 Letellier, M.; Chevallier, F.; Béguin, F.; Frackowiak, E.; Rouzaud, J.-N. The first in situ $^7Li$ NMR study of the reversible lithium insertion mechanism in disorganised carbons. *J. Phys. Chem. Solids* **2004**, *65*, 245–251.

17 Tarascon, J.-M.; Gozdz, A. S.; Schmutz, C.; Shokoohi, F.; Warren, P. C. Performance of Bellcore's plastic rechargeable Li-ion batteries. *Solid State Ionics* **1996**, *86–8*, 49–54.

18 Letellier, M.; Chevallier, F.; Béguin, F. In situ $^7Li$ NMR during lithium electrochemical insertion into graphite and a carbon/carbon composite. *J. Phys. Chem. Solids* **2006**, *67*, 1228–1232.

19 Letellier, M.; Chevallier, F.; Morcrette, M. In situ $^7Li$ nuclear magnetic resonance observation of the electrochemical intercalation of lithium in graphite; 1st cycle. *Carbon* **2007**, *45*, 1025–1034.

20 Key, B.; Bhattacharyya, R.; Morcrette, M.; Seznéc, V.; Tarascon, J.-M.; Grey, C. P. Real-time NMR investigations of structural changes in silicon electrodes for lithium-ion batteries. *J. Am. Chem. Soc.* **2009**, *131*, 9239–9249.

21 Bhattacharyya, R.; Key, B.; Chen, H. L.; Best, A. S.; Hollenkamp, A. F.; Grey, C. P. In situ NMR observation of the formation of metallic lithium microstructures in lithium batteries. *Nat. Mater.* **2010**, *9*, 504–510.

22 Trease, N. M.; Zhou, L.; Chang, H. J.; Zhu, B. Y.; Grey, C. P. In situ NMR of lithium ion batteries: Bulk susceptibility effects and practical considerations. *Solid State Nucl. Magn. Reson.* **2012**, *42*, 62–70.

23 Zhou, L.; Leskes, M.; Leskes, M.Trease, N. M.Grey, C. P. Paramagnetic Electrodes and Bulk Magnetic Susceptibility Effects in the *in situ* NMR Studies of Batteries: Application to $Li_{1.08}Mn_{1.92}O_4$ Spinels. *J. Magn. Reson.* **2013**, in press, http://dx.doi.org/10.1016/j.jmr.2013.05.011.

24 Wang, H.; Koester, T. K.-J.; Trease, N. M.; Ségalini, J.; Taberna, P.-L.; Simon, P.; Gogotsi, Y.; Grey, C. P. Real-time NMR studies of electrochemical double-layer capacitors. *J. Am. Chem. Soc.* **2011**, *133*, 19270–19273.

25 Poli, F.; Kshetrimayum, J. S.; Monconduit, L.; Letellier, M. New cell design for in-situ NMR studies of lithium-ion batteries. *Electrochem. Commun.* **2011**, *13*, 1293–1295.

26 Slezak, P. J.; Wieckowski, A. Electrode potential dependent NMR spectra of surface $^{13}CO$ on polycrystalline platinum. *J. Electroanal. Chem.* **1992**, *339*, 401–410.

27 Han, O. H. Nuclear magnetic resonance investigations on electrochemical reactions of low temperature fuel cells operating in acidic conditions. *Prog. Nucl. Magn. Reson. Spectrosc.* **2013**, *72*, 1–41.

28 Slezak, P. J.; Wieckowski, A. Interfacing surface electrochemistry with solid-state NMR. Characteriztion of surface CO on polycrystalline platinum. *J. Magn. Reson. A* **1993**, *102*, 166–172.

29 Wu, J.; Day, J. B.; Franaszczuk, K.; Montez, B.; Oldfield, E.; Wieckowski, A.; Vuissoz, P. A.; Ansermet, J.-P. Recent progress in surface NMR-electrochemistry. *J. Chem. Soc., Faraday Trans.* **1997**, *93*, 1017–1026.

30 Tong, Y. Y.; Oldfield, E.; Wieckowski, A. Exploring electrochemical interfaces. *Anal. Chem.* **1998**, *70*, 518A–527A.

31 Day, J. B.; Vuissoz, P.-A.; Oldfield, E.; Wieckowski, A.; Ansermet, J.-P. Nuclear magnetic resonance spectroscopic study of the electrochemical oxidation product of methanol on platinum black. *J. Am. Chem. Soc.* **1996**, *118*, 13046–13050.

32 Slichter, C. P. *Principles of Magnetic Resonance*, 3rd ed.; Springer-Verlag: Berlin, 1989; Vol. 1.

33 Yahnke, M. S.; Rush, B. M.; Reimer, J. A.; Cairns, E. J. Quantitative solid-state NMR spectra of CO adsorbed from aqueous solution onto a commercial electrode. *J. Am. Chem. Soc.* **1996**, *118*, 12250–12251.

34 Rush, B. M.; Reimer, J. A.; Cairns, E. J. Nuclear magnetic resonance and voltammetry studies of carbon monoxide adsorption and oxidation on a carbon-supported platinum fuel cell electrocatalyst. *J. Electrochem. Soc.* **2001**, *148*, A137–A148.

35 Tong, Y. Y.; Wieckowski, A.; Oldfield, E. NMR of electrocatalysts. *J. Phys. Chem. B* **2002**, *106*, 2434–2446.

36 Bucher, J. P.; Buttet, J.; Van Der Klink, J. J.; Graetzel, M.; Newson, E.; Truong, T. B. $^{195}$Pt NMR-studies of supported catalysts. *Colloids Surf.* **1989**, *36*, 155–167.

37 Tong, Y. Y.; van der Klink, J. J. Local metal to non-metal transition on oxygen-covered platinum particles from $^{195}$Pt nuclear magnetic resonance. *J. Phys.: Condens. Matter* **1995**, *7*, 2447–2459.

38 Tong, Y. Y.; Belrose, C.; Wieckowski, A.; Oldfield, E. First observation of platinum-195 nuclear magnetic resonance in commercial graphite-supported platinum electrodes in an electrochemical environment. *J. Am. Chem. Soc.* **1997**, *119*, 11709–11710.

39 Rice, C.; Tong, Y. Y.; Oldfield, E.; Wieckowski, A. Cyclic voltammetry and $^{195}$Pt nuclear magnetic resonance characterization of graphite-supported commercial fuel cell grade platinum electrocatalysts. *Electrochim. Acta* **1998**, *43*, 2825–2830.

40 Paik, Y.; Kim, S.-S.; Han, O. H. Methanol behavior in direct methanol fuel cells. *Angew. Chem., Int. Ed.* **2008**, *47*, 94–96.

41 Wasmus, S.; Küver, A. Methanol oxidation and direct methanol fuel cells: A selective review. *J. Electroanal. Chem.* **1999**, *461*, 14–31.

42 Han, O. H.; Han, K. S. Toroidal Probe Unit for Nuclear Magnetic Resonance. U.S. Patent 7,339,378, 2006.

43 Han, O. H.; Han, K. S.; Shin, C. W.; Lee, J.; Kim, S.-S.; Um, M. S.; Joh, H.-I.; Kim, S.-K.; Ha, H. Y. Observation of methanol behavior in fuel cells in situ by NMR spectroscopy. *Angew. Chem., Int. Ed.* **2012**, *51*, 3842–3845.